Towards a Population-Based Approach for Dynamic Monitoring of Underground Structures: A Numerical Study on Metro Tunnel Models

infrastructures

MDPI

Article

Towards a Population-Based Approach for Dynamic Monitoring of Underground Structures: A Numerical Study on Metro Tunnel Models

Giulia Delo *, Camilla Corbani and Cecilia Surace

Department of Structural, Geotechnical and Building Engineering, Politecnico di Torino, Corso Duca degli Abruzzi, 24, 10129 Torino, Italy
* Correspondence: giulia.delo@polito.it

Abstract

Underground structures are becoming increasingly vital components of modern transportation networks and urban systems, making their structural integrity a critical factor for safety and operational reliability. However, despite considerable progress in Structural Health Monitoring (SHM), the application of data-driven and vibration-based strategies to underground infrastructures remains an open and under-explored field, often because of limited data availability. Population-Based Structural Health Monitoring (PBSHM) offers a promising pathway to overcome this challenge by leveraging transfer learning to share diagnostic knowledge among similar structures. This study investigates the feasibility of extending the PBSHM paradigm to underground infrastructures, with a particular focus on a metro tunnel application. Through dynamic finite element simulations, relevant vibration features are identified, and damage detection strategies based on transmissibilities and cross-correlation functions are evaluated. The numerical results show that transmissibility-based indicators enable accurate damage localisation along the tunnel lining, even under noisy conditions. In contrast, cross-correlation features exhibit more limited performance in some configurations. Building on this evidence, the transmissibility-based damage indicator is subsequently embedded within the PBSHM framework and used as a transferable feature between tunnel models, achieving reliable damage detection in a second tunnel with heterogeneous characteristics, with F1 scores exceeding 80% for all considered damage severities and above 94% for the most critical case, thereby highlighting the potential of knowledge transfer for large-scale underground networks.

Keywords: underground structures; structural health monitoring; knowledge transfer; domain adaptation

Academic Editors: Yunhao Dong and Tong Zhang

Received: 8 January 2026
Revised: 17 February 2026
Accepted: 25 February 2026
Published: 28 February 2026

1. Introduction

Many large cities and metropolitan areas are facing a progressive increase in urban traffic, which poses significant challenges in managing mobility and ensuring the efficiency of transportation networks. As a result, underground infrastructures have become crucial components in densely populated areas [1]. Although underground spaces—such as metro tunnels—have long been used for public transportation, the recent decades have seen the design and construction of numerous new facilities, leading to a continuous expansion of underground mileage. Metro tunnel networks not only alleviate surface traffic congestion but also offer several advantages, including the capacity to handle

high passenger volumes, reduced vulnerability to adverse weather conditions, and the capability to connect areas with diverse morphological characteristics [2]. Nevertheless, the construction and management of these structures remain complex, requiring careful consideration of the interaction with the surrounding soil, which often constitutes a harsh and variable environment. In addition, the growing number of recently constructed tunnels and the progressive ageing of the ones that have been in service for years require careful verification of their structural conditions to ensure efficient service and user safety.

1.1. SHM of Underground Infrastructures

A variety of Structural Health Monitoring (SHM) strategies have been developed for underground infrastructures; however, most existing studies concentrate on static approaches, whereas dynamic-based techniques remain comparatively limited.

The development of deformations and cracks in tunnel linings has been extensively analysed in both concrete and masonry structures [3–5]. Many of these static approaches are based on Distributed Fiber Optical Sensors (DFOS) and Fiber Bragg Grating (FBG) to monitor deformations and strains [6]. Gòmez et al. (2020) show in [7] how DFOS has good potential, associated with post-processing algorithms, to become a reliable tool for strain monitoring in tunnels influenced by the construction of nearby buildings; similarly, in [5], DFOS were adopted to detect local strains and cracks in an old masonry tunnel structure caused by nearby tunnelling activity, confirming its certain effectiveness. The validity of DFOS in hostile environments, and in hard-to-reach locations, has been evaluated in [8] by Di Murro et al. (2019), where these sensors were used for the remote static monitoring of tunnels in the presence of radiation. Then, Wang et al. (2023) [3] exploited the DFOS and FBG sensor technologies to monitor steel-fibre-reinforced concrete behaviour in a scaled experimental model of tunnel lining segments, detecting the strains at different stages. Moreover, FBG have been exploited in [9,10] to monitor strain and temperature variations in tunnel linings, and Tondini et al. (2015) [11] employed different systems of FBG sensors to evaluate the inelastic response of concrete tunnel lining under seismic actions.

Several non-contact approaches have also been proposed. For instance, Terrestrial Laser Scanning (TLS) has been increasingly used to produce accurate 3D representations [12]; its use has been associated with photogrammetry methods to assess cracks and water seepage in a tunnel structure in [13], showing a good performance of these two visual perception methods. Additionally, some studies proposed machine learning and deep learning methods aimed at improving damage detection and prediction accuracy. Ouyang et al. (2023) [14] proposed a robot-mounted imaging technology to detect cracks in tunnel linings, adopting transfer learning methods; while in [15], image data have been collected by an automated monitoring system and elaborated by deep learning algorithms to identify cracks.

Conversely, few investigations have been executed using vibration-based techniques. Zhou et al. (2014) [16] expressed the open challenges in applying dynamic monitoring to underground structures by comparing the vibration characteristics of the tunnel–soil coupled system and those of the free tunnel, providing a Timoshenko Beam–Transfer Matrix Method; subsequently, the author studied the vibration characteristics of a metro station underneath a high-speed railway by performing field tests and trying to separate the underground structure's modal components to those of the surrounding soil [17]. Yan et al. (2021) [18] evaluated the structural safety of tunnels during the construction phase using dynamic monitoring data, comparing the simulation results to those of an actual case study and estimating the failure probability during construction. Feng et al. (2015) [1] tested the feasibility and accuracy of Transmissibility and Cross-correlation functions as sensitive features for damage localisation on a finite element model of a tunnel structure under different

types of damage, finding reliable results. Some studies also integrated machine learning methods in dynamic SHM. For instance, a deep learning algorithm has been applied to the data gathered from a finite element model of a metro tunnel subjected to varying damage intensities to monitor the vibrations induced by a moving load [19]. Nevertheless, the strong interaction between the tunnel structure and the surrounding soil must be carefully accounted for to obtain reliable estimates [16]. Beyond the specific context of tunnels, recent research has extensively investigated structural damage identification using optimisation and deep learning techniques. Swarm intelligence algorithms, such as Sailfish Optimisation (SFO), have been employed in two-stage identification schemes for bridge bearings, where element-wise damage parameters are inferred by minimising discrepancies in modal quantities or relative modal strain energy [20]. Similarly, Moth–Flame Optimisation (MFO) has been adopted for the localisation and quantification of damage, exploiting modal strain energy and static displacements [21]. Several studies have likewise explored deep-learning-based strategies for distinct SHM applications. Convolutional neural networks have been applied to time–frequency representations of acceleration signals to detect and localise damage in steel and concrete structures under varying environmental conditions, often achieving improved classification performance compared with traditional feature-based approaches [22]. Although these damage-identification methods have demonstrated promising results across a range of structural applications, their implementation in underground structures and metro tunnels remains limited.

Furthermore, the adoption of data-driven approaches for SHM becomes particularly challenging when comprehensive datasets are unavailable. This limitation can be mitigated through the recently introduced Population-Based Structural Health Monitoring (PBSHM) framework [23].

1.2. The PBSHM Framework

Traditional SHM methodologies are typically designed for individual structures, and even when machine learning algorithms are employed, the predictive model is generally trained and updated using data collected exclusively from that structure. The PBSHM framework addresses this constraint by enabling knowledge transfer among a population of similar assets, using the available information from a well-instrumented source structure to infer the condition of a target structure with limited or missing data. A broad overview of PBSHM fundamentals is provided in [23–25], where the authors introduce the overall strategy and the notion of structural populations, and distinguish between homogeneous and heterogeneous populations according to their level of similarity.

In a homogeneous population, the structures are identical in terms of geometry, materials, boundary conditions, and topology, so that any differences in their dynamic responses can be mainly attributed to damage or operational variability. In a heterogeneous population, by contrast, the members exhibit systematic differences in one or more attributes (such as stiffness, mass distribution, cross-sectional layout, support conditions, or overall configuration), and these differences must be explicitly accounted for when comparing or transferring information across the population.

Consequently, PBSHM requires methods to assess structural similarities, typically relying on the Irreducible Element (IE) representation of a structure. The IE representation, introduced in [24], is constructed to retain only those properties and dimensions that strongly influence knowledge transfer; it abstracts the relevant features of a structure into a reduced set of main components with well-understood dynamic behaviour, thereby simplifying the understanding of the system and the identification of feasible levels of inference between population members. The aspects expressed in an IE, typically arranged in tabular form, can then be graphically represented in a corresponding Attribute Graph (AG),

which facilitates automatic graph-comparison procedures and the systematic assessment of similarity within the population [26].

Based on the level of similarity within the population, various knowledge-transfer techniques can be employed. Among transfer-learning techniques, domain adaptation (DA) proves to be an ideal fit for PBSHM because it aims to minimise the differences between the features of the source and target structures. Thereby, DA allows adopting the features acquired from a source structure to infer consistent data-driven diagnostics on a new target. The core assumption of DA is that useful knowledge can be transferred from the source to the target domain, even when the corresponding feature distributions differ, by minimising the distance between their statistical representations [27]. This strategy has already been implemented in several engineering domains, including wind turbines [28], bridges [29], and aerospace structures [30,31]. However, its application to underground infrastructures has not yet been explored.

1.3. Research Objectives and Scope

In this study, the feasibility and accuracy of Transmissibility Functions (TFs) and Cross-Correlation Functions (CCFs) are first examined as vibration-based damage-sensitive features for underground structures, using an integrated tunnel–soil finite element model under two different loading conditions. Subsequently, a second tunnel configuration is analysed, and a DA algorithm based on Statistical Alignment (SA) [29] is implemented to assess the potential of the PBSHM framework for heterogeneous underground infrastructures. Despite the aforementioned advances, the main research challenges addressed in this work are summarised as follows:

- Limited use of dynamic, vibration-based SHM for underground structures and metro tunnels.
- Scarcity of labelled monitoring data for individual underground assets.
- Strong tunnel–soil interaction, which complicates the extraction of damage-sensitive dynamic features.
- Lack of established procedures for sharing diagnostic knowledge between different underground structures.

Accordingly, the main contributions of this paper are:

- Numerical assessment of TFs and CCFs as vibration-based damage-sensitive features for tunnel–soil systems.
- Analysis of the proposed damage indicators under measurement noise and realistic testing conditions.
- Integration of transmissibility-based features into a PBSHM framework using domain adaptation, for improving diagnostics in underground structures.

The layout of the paper is as follows. Section 2 presents the finite element simulation of the metro tunnels. Section 3 introduces the adopted damage identification strategies, with a focus on the source structure. Subsequently, Section 4 explores the domain adaptation algorithm used for PBSHM. Lastly, Section 5 presents the discussions and some conclusions.

2. Modelling and Simulation of Metro Tunnel Dynamics

This section outlines the key features of the monitored structure and the development of its finite element model, demonstrating the validity of TF and CCF in damage identification and evaluating the use of a PBSHM approach, where the first structure serves as the source and the second as the target. The undamaged and damaged configurations are modelled and analysed for the damage evaluation. The numerical case study considered in this

work is a metro tunnel, whose geometry, material properties, and modelling assumptions are derived from Feng et al. [1].

2.1. Finite Element Approach for Tunnel Analysis

The finite element (FE) model developed for the source structure, using the *ANSYS Mechanical APDL* 2021 R1 software, is first presented. Since the case study focuses on metro tunnels, the interaction between the tunnel and the surrounding soil is explicitly considered by constructing an integrated tunnel–soil system. The corresponding tunnel geometry is depicted in Figure 1.

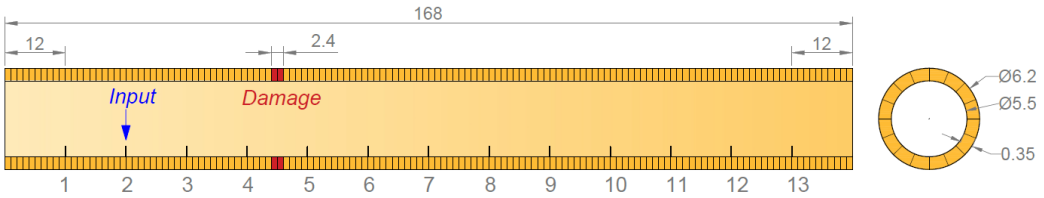

Figure 1. First tunnel geometry and sensors. The tunnel is divided into segments of length 1.2 m. The gray numbers represent all the possible input and measurement points. In this figure, the input is applied to point 2 (blue arrow) and damage (red segments) occurs between point 4 and point 5 (measures in m; figure not in scale).

The soil domain is represented using a full-circle spring model, following the assumption proposed in [1]; spring elements are therefore introduced in both radial and tangential directions. Specifically, Link180 elements are employed to reproduce the soil's radial stiffness, whereas Combin14 elements simulate its tangential response. Link180 elements are three-dimensional spar elements with three degrees of freedom (DOFs) per node, capable of sustaining only uniaxial tension–compression behaviour. Conversely, Combin14 elements act as longitudinal spring–damper components with three translational DOFs per node, incapable of bending or torsion. The tunnel lining consists of concrete segments forming a circular cross-section, discretised into sixteen shell elements. The internal and external diameters are 5.5 m and 6.2 m, respectively, corresponding to a wall thickness of 0.35 m. The total longitudinal length of the model is 168 m, with each segment extending 1.2 m. The soil medium is assumed to resist only compressive loads. An elastic modulus of 5.06×10^2 MPa is assigned to the Link180 elements, while the Combin14 elements are characterised by a spring constant of 3.0×10^6 N/m. For both element types, the opposite node is fixed to represent boundary constraints. Structural damage is simulated by applying a 13% reduction in the concrete elastic modulus over two tunnel sections, representing a localised deterioration scenario and enabling evaluation of the sensitivity of the TFs and CCFs to such damage.

The reduced modulus is assigned to the sixteen shell elements located at longitudinal coordinates $z = 52.8$ m and $z = 54$ m from the reference origin, corresponding to a total damaged length of 2.4 m. The specific damage locations and associated reductions in elastic modulus are reported in Table 1. All remaining material properties, geometric parameters, and modelling assumptions are consistent with those of the undamaged configuration. The complete material properties are summarised in Table 2. In addition, an equivalent viscous damping ratio of 6% is introduced.

Table 1. Damaged concrete (tunnel lining) features.

Initial Elastic Modulus (MPa)	Reduced Elastic Modulus (MPa)	Quotes (z Direction, m)
3.45×10^4	3.0015×10^4	52.8–55.2

Table 2. Concrete and soil properties for the first tunnel structure.

Material	Elastic Modulus [MPa]	Poisson's Ratio	Density (kg/m^3)
Concrete	3.45×10^4	0.2	2551
Damaged concrete	3.0015×10^4	0.2	2551
Soil	5.00	0.3	1836

The updated model for the tunnel–soil coupled system in the undamaged condition is shown in Figure 2.

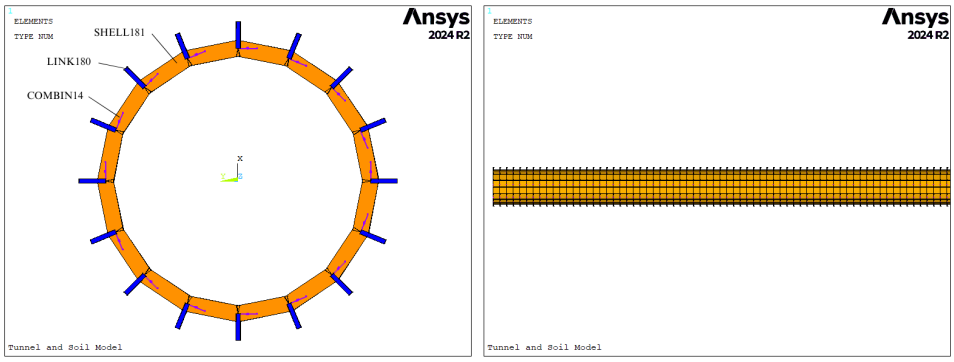

(**a**) (**b**)

Figure 2. The undamaged tunnel–soil coupled system. (**a**) Cross-section. (**b**) Longitudinal view.

An additional tunnel–soil finite element model was developed to represent the second tunnel in healthy and damaged conditions, following the same assumptions of the source structure and including soil–structure interaction through the same radial and tangential spring formulation. This structure is adopted as the target, i.e., a structure for which the measured data are unlabelled and used for the training and testing phases of the transfer learning process. The element discretisation and the soil properties are unchanged, while the geometry and material properties are obtained from [32]: the inner diameter is equal to 5.6 m, and the outer one is 6.2 m, so the wall thickness is 30 cm, and a length of 168 m is considered in the longitudinal direction. Thus, the source and target structures share the same topology and type of damage (a reduction of 13% in the concrete elastic modulus) while exhibiting heterogeneous attributes, as discussed in [26]. Table 3 summarises the material properties.

Table 3. Concrete and soil properties for the second tunnel structure.

Material	Elastic Modulus [MPa]	Poisson's Ratio	Density (kg/m^3)
Concrete	3.62×10^4	0.2	2551
Damaged concrete	3.1494×10^4	0.2	2551
Soil	5.00	0.3	1836

2.2. Simulation of the Experimental Test Procedure

A hammer-impact simulation was performed on both finite element models of the source and target structures to obtain the acceleration responses through transient dynamic analysis. Thirteen measurement points were positioned along the tunnel footing at uniform intervals of 12 m in the longitudinal direction, as illustrated in Figure 1. Two distinct testing configurations were therefore considered to investigate the relevance of vibration-based strategies for tunnel SHM. In the first configuration, a vertical impulsive load was applied at a fixed location (point 2), and the resulting vertical acceleration responses were

recorded at all sensor positions. In the second configuration, the external excitation was sequentially applied to each section $(i+1)$, while acceleration responses were measured only at the adjacent points i and $(i+1)$. This setup enables the assessment of localised dynamic behaviour while limiting the number of required measurements. Conversely, the fixed-input configuration is introduced here to assess whether an operationally simpler testing scheme, involving a single excitation location and simultaneous measurements at multiple points, can provide damage-identification performance comparable to that of the variable-input configuration. In both simulations, the input force had a duration of 5 ms and a peak magnitude of 4800 N, consistent with hammer-impact models used in comparable experimental studies. A sampling frequency of 800 Hz and a total measurement duration of 4.5 s were adopted. Representative acceleration responses at locations 1 and 2 resulting from an impact at point 2 are presented in Figure 3.

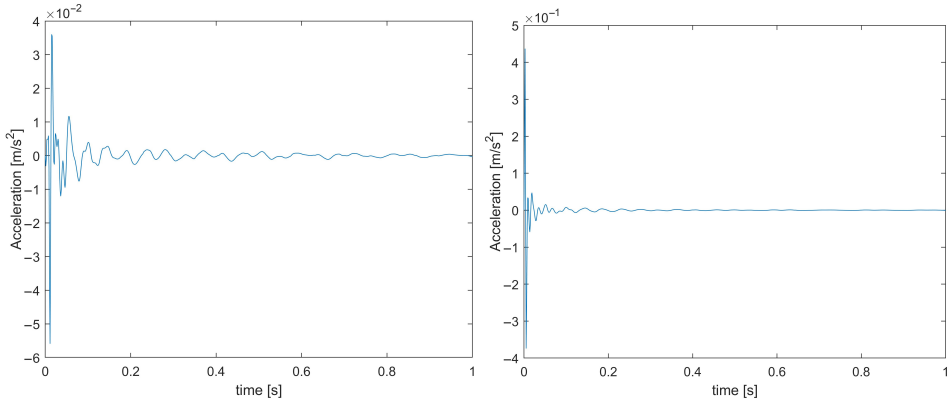

(**a**) (**b**)

Figure 3. Acceleration time histories for external input at location 2 in the undamaged model (truncated signals). (**a**) Measurement point n.1. (**b**) Measurement point n.2.

The sampling frequency and the duration of the test are summarised in Table 4. The input is applied for a time $T_{imp} = 0.005$ s by incremental steps of $\Delta t = 0.00125$ s, whereas the acceleration responses are gathered every $\Delta t = 0.00125$ s for a total time of $T_{tot} = 4.5$ s after the application of the external load. The selected parameters satisfy both the Nyquist-Shannon theorem and the stability criterion.

Table 4. Solution settings.

Quantity	Value	Units
Sampling frequency f_s	800	Hz
Sampling time Δt	0.00125	s
Input duration T_{imp}	0.005	s
Test duration T_{tot}	4.5	s

3. Damage Identification Strategies and Results

This section presents the vibration-based damage identification strategies adopted for the tunnel–soil system, together with the corresponding numerical results. Two scalar indices are considered, namely a Transmissibility-based Damage Indicator (TDI) and a Cross-correlation-based Damage Indicator (CDI), which are both directly derived from measurable acceleration responses. These features were identified on the basis of the previously outlined review of vibration-based SHM methods for underground structures, which highlighted transmissibility and cross-correlation functions as among the most promis-

ing candidates for detecting local stiffness reductions in tunnel linings while remaining compatible with practical monitoring layouts.

The forced vibration problem of a viscously damped n-degrees of freedom (DOF) system is ruled by the equation $\mathrm{M}\ddot{x}(t) + \mathrm{C}\dot{x}(t) + \mathrm{K}x(t) = \mathrm{f}(t)$, in which $\mathrm{M}, \mathrm{K}, \mathrm{C}$ are the mass, stiffness and damping matrices, respectively, $x(t)$ is the displacement vector and $\mathrm{f}(t)$ is the load vector. The TF between two DOFs i and j, for the external load applied in the k^{th} DOF, is evaluated as $T_{ij(k)}$.

$$T_{ij(k)}(\omega) = \frac{\mathrm{A_{i(k)}}(\omega)}{\mathrm{A_{j(k)}}(\omega)} = \frac{-\omega^2 \mathrm{H_{i(k)}}(\omega)\mathrm{F_k}(\omega)}{-\omega^2 \mathrm{H_{j(k)}}(\omega)\mathrm{F_k}(\omega)} = \frac{\mathrm{H_{i(k)}}}{\mathrm{H_{j(k)}}} \tag{1}$$

where $\mathrm{A_{i(k)}}$ and $\mathrm{A_{j(k)}}$ are the acceleration spectra of DOFs i and j respectively (obtained by deriving the displacement spectra twice), and $\mathrm{H_{i(k)}}(\omega)$ and $\mathrm{H_{j(k)}}(\omega)$ are their Frequency Response Functions (FRFs). By defining the TF as the ratio of two spectral accelerations, Equation (1) shows that the assessment of this feature does not require measuring the external input or the FRF, which makes it particularly advantageous for applications in SHM. The TDI between DOFs i and j, for the external input applied in k, is defined as:

$$TDI_{ij(k)} = \frac{\int_{\omega_1}^{\omega_2} |\log|T^U_{ij(k)}| - \log|T^D_{ij(k)}|| \, d\omega}{\int_{\omega_1}^{\omega_2} |\log|T^U_{ij(k)}|| \, d\omega} \tag{2}$$

where ω_1 and ω_2 define the frequency range of interest, and $T^U_{ij(k)}$ and $T^D_{ij(k)}$ identify the TF for the undamaged and damaged conditions, respectively. Hence, this indicator is constructed to condense the frequency-dependent discrepancies between the transmissibility functions of the undamaged and damaged configurations into a single scalar quantity over a prescribed frequency band.

The second damage identification algorithm is the CCF; considering the DOFs i and j of the previous n-DOFs system, the CCF can be computed from their acceleration responses $\ddot{x}_i(t)$ and $\ddot{x}_j(t)$:

$$R_{i,j}(\tau) = \lim_{T\to\infty} \frac{1}{T} \int_0^T \ddot{x}_i(t)\ddot{x}_j(t+\tau) \, dt \tag{3}$$

where τ is the time lag applied to the second signal. The CCF can be normalised with respect to the zero-lag autocorrelation functions. Hence, the CDI is given by Equation (4), where superscript U and D denote the normalised CCFs in undamaged and damaged conditions, respectively.

$$CDI_{ij} = \frac{\sum_{k_1}^{k_2} ||\widetilde{R}^D_{ij}| - |\widetilde{R}^U_{ij}||}{\sum_{k_1}^{k_2} |\widetilde{R}^U_{ij}|} \tag{4}$$

Similarly to TDI, it is important to assess the CDI at various locations within the structure. In both cases, damage localisation is carried out by analysing the spatial distribution of the indicator values and identifying the position along the tunnel at which the indicator attains its maximum. The damage location is therefore associated with the sensor pair (or section) corresponding to the highest value of the selected damage indicator.

3.1. Fixed Input Location Test

The following section presents the results obtained from the fixed-input test on the source structure. In these simulations, the hammer excitation was applied at position 2, and damage was expected to occur between positions 4 and 5. The frequency range of 5–40 Hz was selected for the application of Equation (2), on the basis of the FRF and modal analyses, which indicated that the main modal contributions are concentrated within this interval, whereas very low and very high frequencies are predominantly associated with

soil-dominated or noise-prone contributions [1]. Conversely, a time window of 0.15–0.35 s was adopted for the CDI, after inspection of the acceleration responses and cross-correlation functions, in order to exclude the immediate impact transient and the late-time decay and to focus on the portion of the response where damage-induced modifications are most evident.

Figure 4a shows the transmissibility functions between measurement points 1 and 2 for the undamaged and damaged configurations, under a hammer impact applied at position 2. The plot highlights the frequency-dependent discrepancies induced by the local stiffness reduction in the lining, while Figure 4b shows the corresponding values of the TDI computed for each same-sensor pair. These results outline that damage can be distinctly identified by the TDI between sensors 4 and 5, where the index attains its maximum value. Conversely, the CDI, as shown in Figure 5, fails to provide a reliable localisation, exhibiting irregular values across several sensor pairs. As a result, its validation was not achieved for the fixed-input configuration at position 2 within the specified time range.

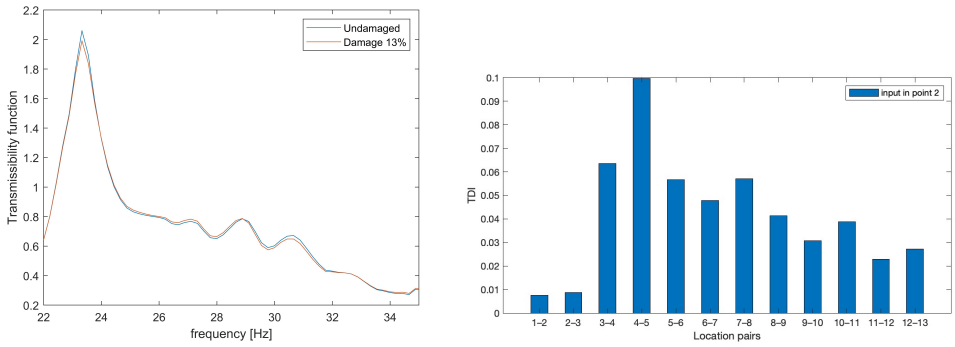

(**a**) (**b**)

Figure 4. Transmissibility functions and TDIs for fixed input in location 2. (**a**) Transmissibility functions T_{12}. (**b**) TDIs: the TDI attains its highest value at the sensor pair corresponding to the damaged section, confirming a correct localisation.

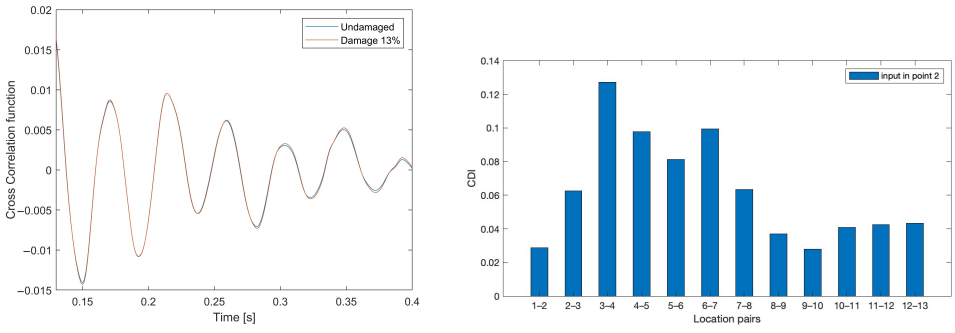

(**a**) (**b**)

Figure 5. Cross-correlation functions and CDIs for fixed input in location 2. (**a**) Cross-correlation functions R_{12}. (**b**) CDIs: the CDI attains its highest value at the sensor pair 3–4, failing to localise the damage.

3.2. Variable Input Location Test

The following section reports the results obtained from the variable-input test on the same structure. The frequency and time ranges of interest remained 5–40 Hz for the TDI and 0.15–0.35 s for the CDI, respectively. Figures 6 and 7 indicate that both damage indices successfully identify and localise the damaged region, with the highest responses observed between sensors 4 and 5, even though the CDI exhibits a broader spatial response with non-negligible values at neighbouring sensor pairs. Moreover, a comparison between the TF and CCF plots for sensor pairs 1–2 and 4–5 highlights that the TF exhibits more pronounced

discrepancies between the healthy and damaged states, which can be attributed to the closer proximity of the latter pair to the damaged zone.

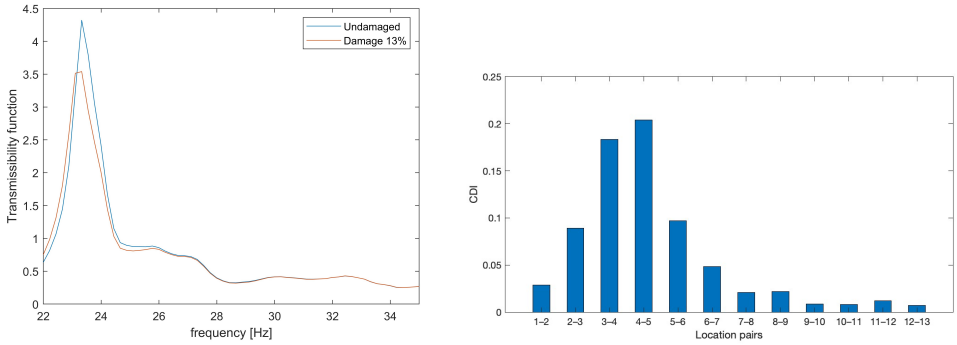

(**a**) (**b**)

Figure 6. Transmissibility functions and TDIs for mobile input location. (**a**) Transmissibility functions T_{45}. (**b**) TDIs: the TDI attains its highest value at the sensor pair corresponding to the damaged section, confirming a correct localisation.

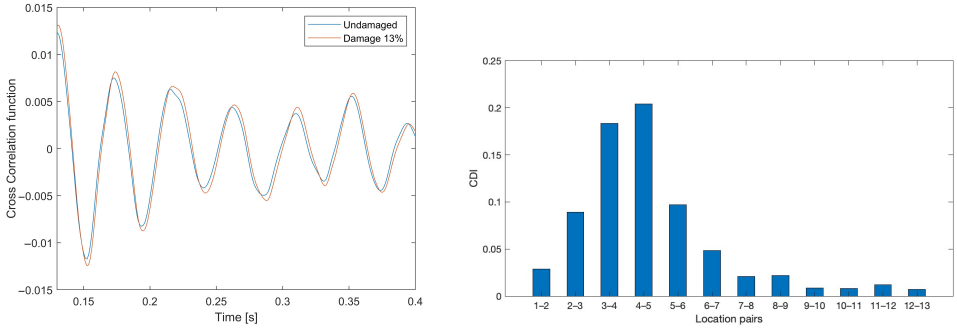

(**a**) (**b**)

Figure 7. Cross-correlation functions and CDIs for mobile input location. (**a**) Cross-correlation functions R_{45}. (**b**) CDIs: the CDI attains its highest value at the sensor pair corresponding to the damaged section, confirming a correct localisation despite the smoother variation of the indicator along the tunnel.

It can be reported that the choice of the frequency range can lead to more or less optimal TDI results. Hence, a modification of this strategy, based on the method of occurrence [33], has been implemented to reduce the variability of the outcomes and to obtain more stable damage-localisation patterns. Indeed, the method of occurrence is used here as a post-processing strategy applied to the frequency-dependent transmissibility-based damage features in order to improve damage localisation by reducing spurious peaks. For each excitation configuration, the absolute difference between the transmissibility functions of the undamaged and damaged models is first evaluated at all sensor pairs and at each frequency line within the selected band. At a given frequency, the sensor pair exhibiting the largest difference is identified and one "occurrence" is assigned to that location. By repeating this procedure over all frequency lines, an occurrence count is obtained for each sensor pair, corresponding to the number of frequencies at which that pair is the most sensitive to damage. The results are shown in Figure 8, which demonstrates effective damage localisation in both fixed and mobile input locations, with a notable improvement in the TDI as false peaks are significantly reduced. In particular, the occurrence-based damage patterns clearly highlight the sensor pair closest to the damaged section, while highlighting significantly spurious responses at other locations, thus enhancing the robustness and interpretability of the TDI for damage detection within the 333 knowledge-sharing framework.

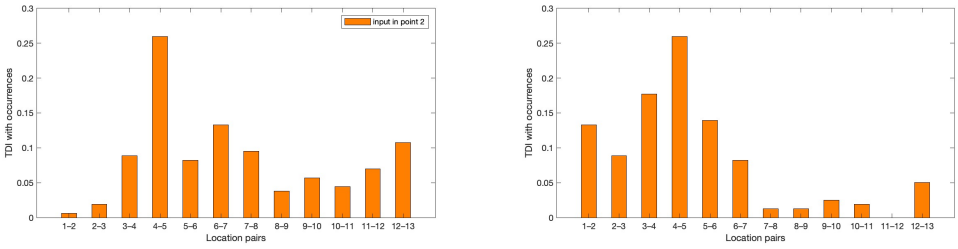

(**a**) (**b**)

Figure 8. TDIs with method of occurrences. (**a**) TDIs for fixed input in location 2. (**b**) TDIs for mobile input location.

These tests demonstrate effective damage localisation in both fixed and mobile input locations, with a notable improvement in the TDI as false peaks are significantly reduced.

3.3. Noise Effects on the Damage-Identification Process

Additional analyses were conducted to further assess the effectiveness of the proposed damage identification approaches, focusing on their robustness to measurement noise under loading condition 2 (mobile input location). This investigation aimed to replicate realistic testing scenarios, in which the recorded acceleration responses are typically affected by random fluctuations, systematic errors, and background noise. Accordingly, the same undamaged and damaged configurations were retained, while Gaussian-distributed noise with varying intensities (0.1%, 1%, and 3%) was superimposed on the acceleration signals. These noise levels were chosen to represent a range of practical measurement conditions, from almost noise-free environments to moderately noisy scenarios, while remaining consistent with noise intensities adopted in previous numerical studies on tunnels, such as [1].

The maximum values of both TDI and CDI in Figure 9 remain located at the sensor pair corresponding to the damaged region, demonstrating a high level of robustness to the three noise levels.

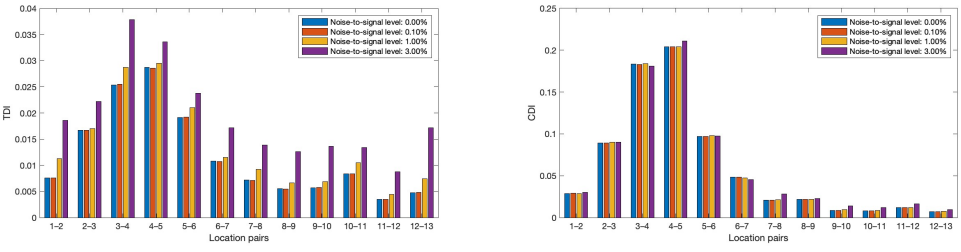

(**a**) (**b**)

Figure 9. TDI and CDI for mobile input location under different noise levels. (**a**) TDIs: the TDI attains its highest value at the sensor pair corresponding to the damaged section, confirming a correct localisation. (**b**) CDIs: the CDI attains its highest value at the sensor pair corresponding to the damaged section, confirming a correct localisation.

4. PBSHM for Underground Structures

Since these vibration-based features demonstrated both sensitivity to damage and generalisable behaviour across comparable structures, the present work explores their integration within the PBSHM framework, employing Statistic Alignment (SA) for information transfer between structural models. The adoption of SA is justified by the high degree of similarity between the analysed structures, which differ only in selected geometric and material parameters [34].

Whereas the previous analysis concentrated solely on damage localisation through pairwise comparisons of transfer functions, the resulting TDI values did not provide information on the presence of damage or on the definition of an anomaly detection threshold. This limitation is addressed by leveraging supplementary knowledge from a suitable source domain. Within this framework, the first tunnel–soil finite element model introduced in Section 2 is treated as the source structure, for which labelled datasets in healthy and damaged conditions are available and can be used to train and calibrate the diagnostic model. The second tunnel–soil finite element model, characterised by different geometric and material properties but the same topology and damage pattern, is treated as the target structure, for which only limited, nominally healthy data are assumed to be available. The motivation for this extension lies in the intrinsic limitations of conventional SHM methods, which typically require labelled datasets representing both damaged and undamaged structural conditions. In real-world applications—particularly for underground infrastructures—such comprehensive datasets are rarely available due to the difficulties associated with direct inspection and controlled experimentation. Within this context, PBSHM enables the exploitation of transferable diagnostic knowledge, thereby reducing the dependency on complete datasets for individual assets. This strategy facilitates damage inference in a target structure by using information obtained from a source structure, which is particularly advantageous for large-scale underground networks where only partial monitoring is feasible.

The analysis was conducted under a fixed-input configuration, using $T_{45(2)}$ to perform the damage detection task. Datasets were expanded via data augmentation, incorporating the previously defined TFs affected by Gaussian noise at a 1% noise-to-signal ratio. This approach aims to evaluate whether features extracted from a reference tunnel can be effectively adapted to a different, yet similar, configuration while preserving their diagnostic sensitivity and reliability.

The SA procedure consists of two main variants: the Normal Condition Alignment (NCA) and the Normal Correlation Alignment (NCORAL) [29]. In this study, the NCA approach was implemented, which performs translation and scaling operations on the target features to minimise their statistical discrepancy from the source domain. This alignment process assumes that the main differences between domains arise from geometric or material variations rather than from damage effects, thus allowing the transfer of meaningful diagnostic information. The source dataset comprised the feature set $X_S = x_1, x_2, \ldots, x_k \in \chi_S$ and corresponding labels Y_S, where $k = 100$ represents the total number of samples, evenly distributed between undamaged ($y = 0$) and damaged ($y = 1$) conditions. The training process additionally included 25 undamaged samples ($y = 0$) from the target domain, $X_T = x_1, x_2, \ldots, x_l \in \chi_T$, while a balanced subset of 50 target-domain samples was reserved for testing. The knowledge-sharing scheme is represented in Figure 10.

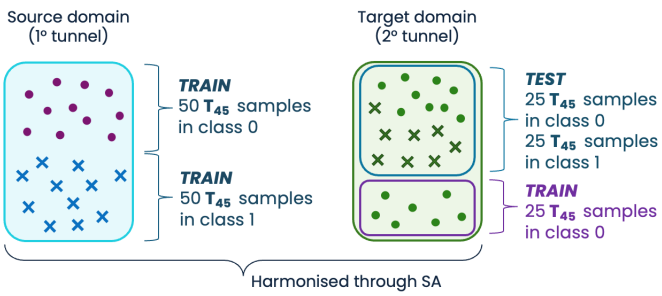

Figure 10. Knowledge-sharing scheme representing the source and target domains and their subsets.

The NCA computes the means and standard deviations of undamaged samples—denoted as $\mu_{s,n}$, $\sigma_{s,n}$, $\mu_{t,n}$, and $\sigma_{t,n}$—and applies the transformation described in Equation (5) to the entire dataset.

$$z_t^{(j)} = \frac{x_t^{(j)} - \mu_{t,n}}{\sigma_{t,n}} \times \sigma_{s,n} + \mu_{s,n} \tag{5}$$

Following SA, the TDIs were computed with respect to the undamaged source samples. The balanced source dataset also enabled the derivation of a classification threshold using a Support Vector Machine (SVM) algorithm with a radial basis function (RBF) kernel to distinguish between damaged and undamaged test samples. The balanced source dataset, comprising 50 undamaged and 50 damaged samples from the source tunnel, was used to train the SVM, while 25 undamaged samples from the target tunnel were included in the SA step but not in the classifier training. The decision boundary was determined on the source-domain data, and the resulting model was then directly applied to the aligned target-domain features without further retraining. The outcomes of the proposed methodology are presented in Figure 11, with the reported results averaged over 100 repetitions to enhance statistical robustness.

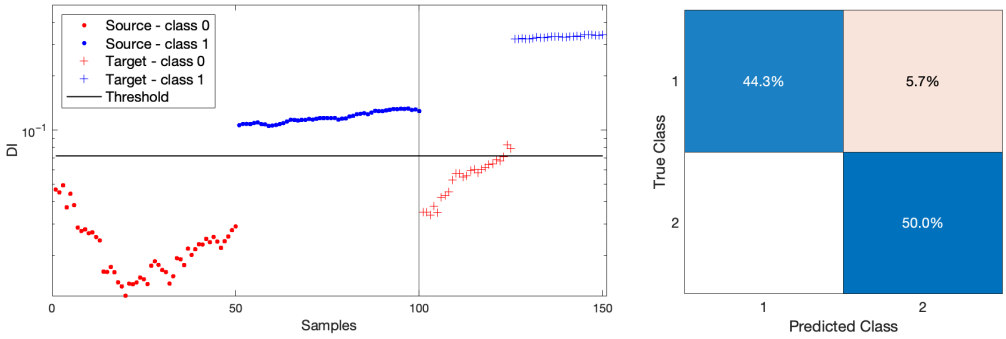

(**a**) (**b**)

Figure 11. Damage-detection performance on the second metro-tunnel after domain adaptation. (**a**) Damage indicators on the test set. (**b**) Confusion matrix.

Figure 11a displays the values of the DI for the source domain, used for training, and the values of the DI computed for the target-domain test set, together with the SVM decision threshold learned from the source data. Each point represents an individual sample, coloured according to its true class (undamaged or damaged), so that the separation induced by the classifier can be directly visualised. Figure 11b reports the corresponding confusion matrix for the target tunnel, obtained by aggregating the classification results over all repetitions.

The obtained results, reported in terms of F_1 score and recall, indicate that the proposed PBSHM approach, supported by SA, allows for consistent and reliable damage detection in the target tunnel even under limited data availability. In particular, the recall measures the proportion of damaged samples that are correctly identified by the classifier, while the F_1 score represents the harmonic mean of precision and recall, thus combining the effects of missed detections and false alarms into a single indicator. This finding supports the potential scalability of the framework to other underground assets, provided that a representative source structure is available. In addition, the method's robustness to mild domain discrepancies suggests that the statistical alignment procedure can effectively compensate for moderate heterogeneity between structures, strengthening the generalisation capability of vibration-based SHM systems. The PBSHM framework was subsequently extended to assess multiple damage scenarios, thereby evaluating the capability of the

proposed approach to detect and classify damages of varying severity. To this end, the target tunnel model was analysed under two additional conditions, involving a 7% and a 9% reduction in the concrete elastic modulus over the same sections illustrated in Figure 1. These configurations were compared with the reference case featuring a 13% stiffness reduction to examine the sensitivity of the method to lower damage intensities. The obtained results, summarised in Table 5, confirm that the model retains satisfactory diagnostic performance even for minor stiffness degradations, thus highlighting the reliability of the proposed strategy.

Table 5. Summary of PBSHM performance under different damage severities.

Damage Level	Reduced Elastic Modulus (MPa)	Detection F1 Score (%)	Recall (%)
13%	3.0015×10^4	94.59	94.88
9%	3.1395×10^4	80.73	81.16
7%	3.2085×10^4	80.73	81.16

5. Discussion and Conclusions

The current study investigates the application of vibration-based and PBSHM methods for monitoring underground structures, testing a DA approach on the numerical models of two metro tunnels. Various hammer impact tests were simulated on the finite element model of the first metro tunnel structure. These tests aimed to demonstrate the sensitivity of TFs and CCFs in identifying damage under different conditions. The results show that the damage indicators presented can accurately locate damage, even in noisy environments. However, both methods are unable to provide knowledge on the presence of damage, as it is not possible to establish a threshold for distinguishing between healthy and damaged conditions. To address this limitation, the study extended the analysis to a PBSHM framework, introducing a second tunnel–soil model to act as the target structure. By leveraging the information learned from the source tunnel, the feasibility of knowledge transfer between heterogeneous underground systems has been explored. The implemented DA strategy, based on SA, effectively reduced the discrepancies between the two models, enabling the transfer of diagnostic knowledge from the source to the target domain. Through this approach, damage detection on the second tunnel has been achieved, establishing a classification threshold derived from the source structure and evaluated via an SVM classifier. The obtained results confirmed strong predictive capability, with an error rate of only 5.7% for misclassified samples and an average accuracy of 94.3% across 100 independent trials. Furthermore, the method was extended to multiple damage scenarios, demonstrating the reliability of the PBSHM approach, even for lower damage intensities. The results confirmed the consistency and sensitivity of TF-based features within the PBSHM framework. Overall, the findings highlight the potential of combining vibration-based features and PBSHM strategies for the SHM of underground infrastructures. TFs proved to be effective not only as direct indicators for vibration-based diagnostics but also as transferable features within a PBSHM context, supporting knowledge generalisation across similar structures. Nevertheless, several aspects require further investigation. The analysis is entirely based on numerical finite element models and relies on a simplified representation of the tunnel–soil interaction, which does not account for all potential behaviours or construction-related irregularities that may arise in real underground environments. Moreover, the excitation is idealised as a hammer impact and does not explicitly consider operational loads, such as train passages or ambient vibrations, so that the performance of the proposed indicators and PBSHM scheme under in-service conditions still needs to be verified. In addition, the proposed framework is applied to a single source–target tunnel pair with limited het-

erogeneity; the extension to higher-dimensional feature sets, more diverse populations of structures, and real monitoring data is therefore left for future work.

Author Contributions: Conceptualization, G.D. and C.S.; Methodology, G.D. and C.S.; Software, G.D. and C.C.; Data curation, G.D. and C.C.; Writing—original draft, G.D.; Writing—review & editing, G.D. and C.S.; Supervision, C.S. All authors have read and agreed to the published version of the manuscript.

Funding: This research received no external funding.

Data Availability Statement: No experimental data were analyzed in this study.

Conflicts of Interest: The authors declare no conflict of interest.

References

1. Feng, L.; Yi, X.; Zhu, D.; Xie, X.; Wang, Y. Damage detection of metro tunnel structure through transmissibility function and cross correlation analysis using local excitation and measurement. *Mech. Syst. Signal Process.* **2015**, *60–61*, 59–74. [CrossRef]
2. Domaneschi, M.; Casciati, S.; Catbas, N.; Cimellaro, G.P.; Inaudi, D.; Marano, G.C. Structural health monitoring of in-service tunnels. *Int. J. Sustain. Mater. Struct. Syst.* **2020**, *4*, 268–291. [CrossRef]
3. Wang, X.; Wang, M.; Jiang, R.; Xu, J.; Li, B.; Wang, X.; Yu, J.; Su, P.; Liu, C.; Yang, Q.; et al. Structural deformation monitoring during tunnel construction: A review. *J. Civ. Struct. Health Monit.* **2023**, *14*, 591–613. [CrossRef]
4. Liu, Z.; Liu, P.; Zhou, C.; Huang, Y.; Zhang, L. Structural Health Monitoring of Underground Structures in Reclamation Area Using Fiber Bragg Grating Sensors. *Sensors* **2019**, *19*, 2849. [CrossRef] [PubMed]
5. Mohamad, H.; Bennett, P.; Soga, K.; Mair, R.; Bowers, K. Behaviour of an old masonry tunnel due to tunnelling-induced ground settlement. *Géotechnique* **2010**, *60*, 927–938. [CrossRef]
6. Zhang, X.; Zhu, H.; Jiang, X.; Broere, W. Distributed fiber optic sensors for tunnel monitoring: A state-of-the-art review. *J. Rock Mech. Geotech. Eng.* **2024**, *16*, 3841–3863. [CrossRef]
7. Gomez, J.; Casas, J.R.; Villalba, S. Structural Health Monitoring with Distributed Optical Fiber Sensors of tunnel lining affected by nearby construction activity. *Autom. Constr.* **2020**, *117*, 103261. [CrossRef]
8. Di Murro, V.; Pelecanos, L.; Soga, K.; Kechavarzi, C.; Morton, R.F.; Scibile, L. Long-term deformation monitoring of CERN concrete-lined tunnels using distributed fibre-optic sensing. *Geotech. Eng. J. SEAGS AGSSEA* **2019**, *50*, 1–7.
9. Barbosa, C.B.; Ferreira, L.A.; Araújo, F.M.; Gonçalves, L.; Gama, C.D.; Malva, R.; Silva, A.; Freitas, V. Fiber Bragg grating system for continuous large-scale monitoring of convergence in Rossio Tunnel. In *Proceedings of the 20th International Conference on Optical Fibre Sensors*; SPIE: Bellingham, WA USA, 2009; Volume 7503, pp. 835–838.
10. Nellen, P.M.; Frank, A.; Broennimann, R.; Sennhauser, U.J. Optical fiber Bragg gratings for tunnel surveillance. In *Proceedings of the Smart Structures and Materials 2000: Sensory Phenomena and Measurement Instrumentation for Smart Structures and Materials*; SPIE: Bellingham, WA USA, 2000; Volume 3986, pp. 263–270.
11. Tondini, N.; Bursi, O.S.; Bonelli, A.; Fassin, M. Capabilities of a Fiber Bragg Grating Sensor System to Monitor the Inelastic Response of Concrete Sections in New Tunnel Linings Subjected to Earthquake Loading. *Comput.-Aided Civ. Infrastruct. Eng.* **2015**, *30*, 636–653. [CrossRef]
12. Wang, W.; Zhao, W.; Huang, L.; Vimarlund, V.; Wang, Z. Applications of terrestrial laser scanning for tunnels: A review. *J. Traffic Transp. Eng. (Engl. Ed.)* **2014**, *1*, 325–337. [CrossRef]
13. Yang, H.; Xu, X. Structure monitoring and deformation analysis of tunnel structure. *Compos. Struct.* **2021**, *276*, 114565. [CrossRef]
14. Ouyang, A.; Di Murro, V.; Cull, M.; Cunningham, R.; Osborne, J.A.; Li, Z. Automated pixel-level crack monitoring system for large-scale underground infrastructure—A case study at CERN. *Tunn. Undergr. Space Technol.* **2023**, *140*, 105310. [CrossRef]
15. Xu, X.; Yang, H. Vision Measurement of Tunnel Structures with Robust Modelling and Deep Learning Algorithms. *Sensors* **2020**, *20*, 4945. [CrossRef]
16. Zhou, B.; Xie, X.Y.; Yang, Y.B.; Jiang, J.C. A novel vibration-based structure health monitoring approach for the shallow buried tunnel. *Comput. Model. Eng. Sci.* **2012**, *86*, 321–348.
17. Zhou, B.; Zhang, F.; Xie, X. Vibration Characteristics of Underground Structure and Surrounding Soil Underneath High Speed Railway Based on Field Vibration Tests. *Shock Vib.* **2018**, *2018*, 3526952. [CrossRef]
18. Yan, X.; Li, H.; Liu, F.; Liu, Y. Structural Safety Evaluation of Tunnel Based on the Dynamic Monitoring Data during Construction. *Shock Vib.* **2021**, *2021*, 6680675. [CrossRef]
19. Abbas, N.; Umar, T.; Salih, R.; Akbar, M.; Hussain, Z.; Haibei, X. Structural Health Monitoring of Underground Metro Tunnel by Identifying Damage Using ANN Deep Learning Auto-Encoder. *Appl. Sci.* **2023**, *13*, 1332. [CrossRef]

20. Huang, M.; Ling, Z.; Sun, C.; Lei, Y.; Xiang, C.; Wan, Z.; Gu, J. Two-stage damage identification for bridge bearings based on sailfish optimization and element relative modal strain energy. *Struct. Eng. Mech. Int. J.* **2023**, *86*, 715–730.
21. Mohamadi Dehcheshmeh, M.; Ghodrati Amiri, G.; Zare Hosseinzadeh, A.; Torbatinejad, V. Structural damage detection based on modal data using moth-flame optimisation algorithm. *Proc. Inst. Civ.-Eng.-Struct. Build.* **2022**, *175*, 79–93.
22. Abdeljaber, O.; Avci, O.; Kiranyaz, S.; Gabbouj, M.; Inman, D.J. Real-time vibration-based structural damage detection using one-dimensional convolutional neural networks. *J. Sound Vib.* **2017**, *388*, 154–170. [CrossRef]
23. Bull, L.A.; Gardner, P.A.; Gosliga, J.; Rogers, T.J.; Dervilis, N.; Cross, E.J.; Papatheou, E.; Maguire, A.E.; Campos, C.; Worden, K. Foundations of population-based SHM, Part I: Homogeneous populations and forms. *Mech. Syst. Signal Process.* **2021**, *148*, 107141. [CrossRef]
24. Gosliga, J.; Gardner, P.A.; Bull, L.A.; Dervilis, N.; Worden, K. Foundations of Population-based SHM, Part II: Heterogeneous populations—Graphs, networks, and communities. *Mech. Syst. Signal Process.* **2021**, *148*, 107144. [CrossRef]
25. Gardner, P.A.; Bull, L.A.; Gosliga, J.; Dervilis, N.; Worden, K. Foundations of population-based SHM, Part III: Heterogeneous populations—Mapping and transfer. *Mech. Syst. Signal Process.* **2021**, *149*, 107142. [CrossRef]
26. Delo, G.; Hughes, A.J.; Surace, C.; Worden, K. On the Influence of Attributes for Assessing Similarity and Sharing Knowledge in Heterogeneous Populations of Structures. *Mech. Syst. Signal Process.* **2025**, *229*, 112554. [CrossRef]
27. Gardner, P.; Liu, X.; Worden, K. On the application of domain adaptation in structural health monitoring. *Mech. Syst. Signal Process.* **2020**, *138*, 106550. [CrossRef]
28. Bull, L.A.; Gardner, P.A.; Rogers, T.J.; Dervilis, N.; Cross, E.J.; Papatheou, E.; Maguire, A.E.; Campos, C.; Worden, K. Bayesian modelling of multivalued power curves from an operational wind farm. *Mech. Syst. Signal Process.* **2022**, *169*, 108530. [CrossRef]
29. Poole, J.; Gardner, P.; Dervilis, N.; Bull, L.; Worden, K. On statistic alignment for domain adaptation in structural health monitoring. *Struct. Health Monit.* **2023**, *22*, 1581–1600. [CrossRef]
30. Delo, G.; Roy, R.; Worden, K.; Surace, C. Using the inverse finite-element method to harmonise classical modal analysis with fibre-optic strain data for robust population-based structural health monitoring. *Strain* **2024**, *61*, e12481. [CrossRef]
31. Delo, G.; Roy, R.; Worden, K.; Surace, C. On the use of the inverse finite element method to enhance knowledge sharing in population-based structural health monitoring. *Comput. Struct.* **2025**, *307*, 107635. [CrossRef]
32. Liu, W.; Wu, X.; Zhang, L.; Wang, Y.; Teng, J. Structural Health-Monitoring and Assessment in Tunnels: Hybrid Simulation Approach. *J. Perform. Constr. Facil.* **2020**, *34*, 04020045. [CrossRef]
33. Devriendt, C.; Presezniak, F.; De Sitter, G.; Vanbrabant, K.; De Troyer, T.; Vanlanduit, S.; Guillaume, P. Structural Health Monitoring in Changing Operational Conditions Using Tranmissibility Measurements. *Shock Vib.* **2010**, *17*, 651–675. [CrossRef]
34. Delo, G.; Bunce, A.; Cross, E.; Gosliga, J.; Hester, D.; Surace, C.; Worden, K.; Brennan, D. When is a Bridge Not an Aeroplane? Part II: A Population of Real Structures. In *Proceedings of the European Workshop on Structural Health Monitoring: EWSHM 2022*; Springer: Cham, Switzerland, 2022; Volume 2, pp. 965–974.